Supplementary Information

Transforming Non-Adhesive Hydrogels to Reversible Tough Adhesives via Mixed-Solvent-Induced Phase Separation

Wei Cui, Ruijie Zhu, Yong Zheng, Qifeng Mu, Menghan Pi, Qiang Chen, and Rong Ran**

Table of contents

Supplementary Methods

***Calculation of polymer volume fraction*:** The as-prepared hydrogels were first swelled in deionized water to achieve swelling equilibrium. Then, the gels were cut into a disk shape with a diameter (d_0) of 15 mm. Afterward, the gels were immersed into organic solvent/water mixtures with varied concentrations of organic solvent ($C_{organic}$, wt%) to reach equilibrium. The diameter (d) of the gels at the equilibrium state in the mixed solvents was measured again. The volume-swelling ratio (Q) of the immersed gels was determined under the assumption of isotropic swelling by:

$$Q = (\frac{d}{d_0})^3 \quad \text{(S1)}.$$

The polymer volume fraction, ϕ, is calculated by:[1]

$$\phi = \frac{\phi_0}{Q} \quad \text{(S2)},$$

where ϕ_0 is the polymer volume fraction of the gels at equilibrium swelling state in water, which can be calculated by utilizing the density of the polymer and water as well as the water content of the gel at equilibrium state.

***90-degree peeling tests*:** The interfacial toughness (Γ), also called the adhesion energy, was measured by the 90-degree peeling tests using a commercial tensile tester (Autograph AG-X, Shimadzu Co., Japan) equipped with a 1 kN load cell in the open atmosphere at room temperature (24 ^{o}C). All hydrogels were cut into a rectangular shape with a dimension of 20 mm in width, 60 mm in length, and 4 to 8 mm in thickness. A stiff tape was attached to the top side of the gel as a backing to prevent the elongation of the gel during the test (**Figure S1**). Before starting the test, partial of the gel was attached to the solid surface and pressed by a weight of 2.5 kg for 5 s. Afterward, the 90-degree peeling tests were performed at a constant

peeling speed of 100 mm min^{-1}. The interfacial toughness, Γ, was determined by dividing the plateau force, F, by the width of the hydrogel, w.[2]

***Uniaxial tensile tests*:** Uniaxial tensile measurements of the hydrogels (width = 2 mm, gauge length = 12 mm, thickness = 1.3 to 2 mm) were performed using an Instron universal test instrument (Model 5576, Instron Instruments, U.S.A.) with a 1 kN load cell at a crosshead velocity of 100 mm min^{-1} at room temperature (24 ^{o}C). The corresponding strain rate is 0.14 s^{-1}. The tensile strain was taken as the change in the length relative to the initial length of the specimen. The elastic modulus (E) was calculated in the initial linear range from the stress-strain curve. The work of extension at fracture (W_{extf}) was defined as the area under the stress-strain curve. For the measurements of hysteresis properties, hydrogels were stretched to a certain strain and then unloaded. The crosshead speed for loading and unloading was fixed at 100 mm min^{-1}. The dissipated energy, U_{hys}, was estimated by the area between the loading-unloading curves by:

$$U_{hys} = \int_{\varepsilon_0}^{\varepsilon} (\sigma_{load} - \sigma_{unload}) d\varepsilon \quad \text{(S3)},$$

where ε_0 and ε are the initial and maximum tensile strain, σ_{load} is the tensile stress during loading, and σ_{unload} is the tensile stress during unloading.

Pure shear Tests: The toughness, T, of the hydrogels was characterized by fracture energy, which was measured according to a classic pure shear experiment.[3] Tests were performed on a commercial tensile tester (Autograph AG-X, Shimadzu Co., Japan) equipped with a 1 kN load cell in the open atmosphere at room temperature. Both notched and unnotched hydrogel samples were used to measure the fracture energy. For the unnotched sample, it was cut into a rectangle shape with a thickness (t) of 1.3 to 2.0 mm, a width (w) of 40 mm, and a length (l) of 60 mm.

The notched sample had the same dimension as the unnotched sample, while a notch of 10 mm in width was initiated from the edge using a razor blade. Both ends of a sample were clamped and displaced at a speed of 100 mm min^{-1} from the initial distance (l_0 = 8 mm) between the clamps. (**Figure S2a**). The unnotched sample was used to measure the stress (σ)-strain (λ) curve, the area beneath which gave the work of extension of the unnotched sample, $W(\lambda)$. The notched sample was used to measure the critical strain, λ_c, at which the notch turned into a running crack (**Figure S2b**). All tests were conducted at room temperature (24 ^oC). During the tests, stress-strain curves of both notched and unnotched samples were recorded. The fracture energy is calculated by:

$$T = W(\lambda_c)l_0 \quad \text{(S4)},$$

where $W(\lambda_c)$ is the work of extension of the unnotched sample at the critical strain, λ_c, where the crack starts to propagate for the notched sample (**Figure S2c**). λ_c was determined by video monitoring.

Rheological tests: The rheological tests on the hydrogels were conducted using an ARES rheometer (Rheometric Scientific Inc.) at room temperature (24 ^oC). The sample was first cut into a cylinder shape with a diameter of 15 mm and a thickness of 1.5 mm, then fixed between metal plates of the rheometer by super glue. To prevent the evaporation of the solvent inside the gel, the sample was surrounded by the organic solvent/water mixture with the $C_{organic}$ in the gel during the measurement. The dynamic strain sweep from 0.01% to 1% was carried out at an angular frequency of 0.14 rad s^{-1} to determine the shear storage modulus (G′) from the linear viscoelasticity region.

Characterization techniques: The polymer surface density of the hydrogels was analyzed by

performing attenuated total reflection Fourier-transform infrared spectroscopy (ATR/FT-IR) on an FT-IR 6600 spectrometer (JASCO, Japan) with diamond prism. Before measurement, the hydrogel was equilibrated in the organic solvent/deuterium oxide mixture that has the same $C_{organic}$ as the original organic solvent/water mixture. Hydrogel spectra were measured in full contact with the prism for wavenumbers of 1800-1000 cm^{-1}. Absorbance maxima, A_{max}, of the characteristic carbonyl group peak ($\upsilon_{C=O}$) for PAAm at 1640 cm^{-1} was determined using the manufacturer software, from which one could compare the variation of polymer surface density of the hydrogels before and after phase separation. Because the gel showed a slightly different volume-swelling ratio in deuterium oxide (D_2O) compared to water, the relative swelling ratio (Q_r) was utilized to calibrate the comparison of the polymer surface density. The Q_r was calculated as:

$$Q_r = \left(\frac{d_{organic/H_2O}}{d_{organic/D_2O}}\right)^3 \quad \text{(S5)},$$

where $d_{organic/H_2O}$ and $d_{organic/D_2O}$ represent the diameter of the same hydrogel equilibrated in the organic solvent/water and organic solvent/deuterium oxide mixtures with the same $C_{organic}$, respectively.

The microstructures of both phase-separated and non-phase-separated hydrogels were examined by a Quanta 250 scanning electron microscope (SEM) (FEI, USA) at an acceleration voltage of 20 kV. First, equilibrated samples were quickly frozen and freeze-dried. Afterward, the freeze-dried samples were fractured carefully, gold-coated, and subjected to the SEM analysis.

Preparation of the freestanding MnO_2 cathode: The used electrolytic manganese dioxide (MnO_2) (EMD, TOSOH, HH-TF 40μm) was obtained from TOSOH company. The MnO_2

cathode was first fabricated by mixing 65 wt% MnO_2 powder, 25 wt% carbon black (ketjen black, KB), and 10 wt% poly(tetrafluoroethylene) (PTFE, suspension, 10 wt%) in ethanol aqueous solution. The freestanding electrode was molded by pressing the mixture in a titanium mesh.

***Preparation of the hydrogel-based battery*:** The gel-based battery was assembled by attaching a zinc foil (Nilaco, thickness 0.2 mm), a piece of calcium chloride ($CaCl_2$)-containing phase-separated (PS) gel, and a freestanding MnO_2 cathode layer by layer. Two pieces of titanium foil were used as current collectors to connect the zinc anode and MnO_2 cathode, respectively. The whole battery was packed in a package made of polyethylene (PE).

Conductivity measurement: The conductivity measurement on the conductive PS gel was conducted on an electrochemistry workstation (Princeton VersaSTAT 3) by using a potentiostatic method. By stretching the gel, the dependence of current on the strain over time was recorded. The direct current (DC) resistance was calculated as:

$$R = \frac{U}{I} \quad \text{(S6)},$$

where R is the DC resistance, U is the applied voltage and I is the monitored current, respectively. For the conductivity measurement on the stretchable conductor that consists of copper sheets bonded by a piece of conductive PS gel, the copper sheets were periodically stretched, which resulted in the strain variation of the PS gel due to the tough gel- solid bonding. The dependence of current on the strain of the conductor over time was recorded, and the DC resistance was also calculated by **Equation (S6)**.

Electrochemical measurements: The galvanostatic discharge test on the conductive PS gel-based battery was carried out on a battery tester (HJ1020SD8 Hokuto Denko) at room

temperature. Electrochemical impedance spectra (EIS) were measured on an electrochemistry workstation (Princeton, VersaSTAT 3) with a frequency range of 100 kHz to 0.1 Hz.

Supplementary Figures and Table

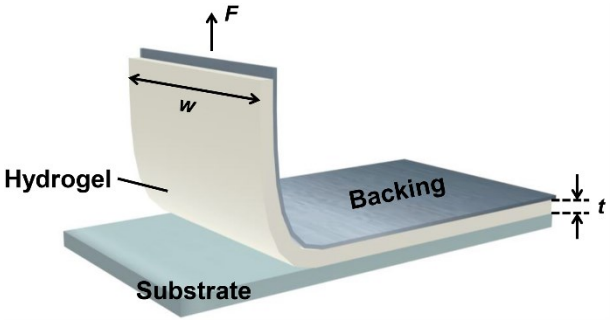

Figure S1. Experimental setup for the 90-degree peeling test. Mechanical testing machine pulls the hydrogel sheet together with a stiff backing in a 90-degree angle from the substrate.

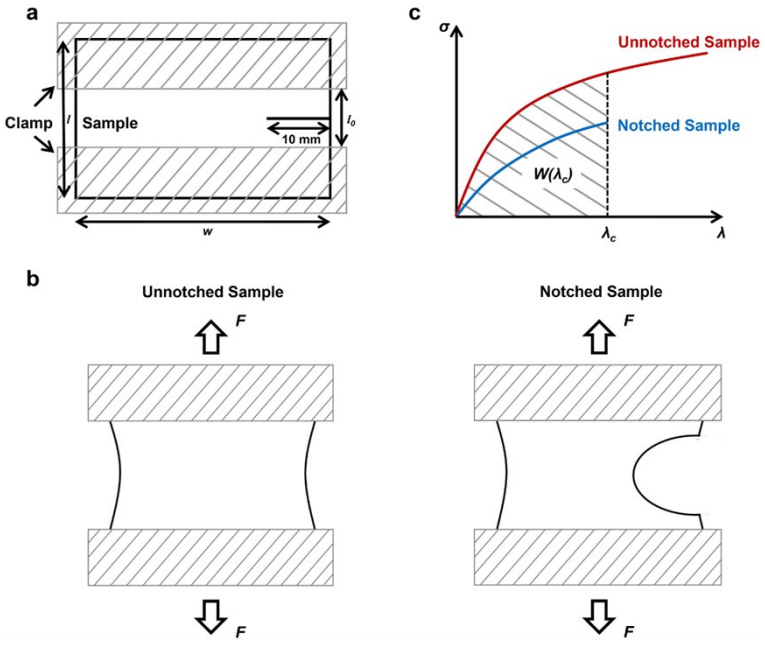

Figure S2. Illustration of the pure shear test to determine the fracture energy. (a) The geometry of a notched sample for the pure shear test. (b) Two gel samples tested in tension. One sample was unnotched, the other sample was notched. (c) The stress (σ)-strain (λ) curves of both samples during the test.

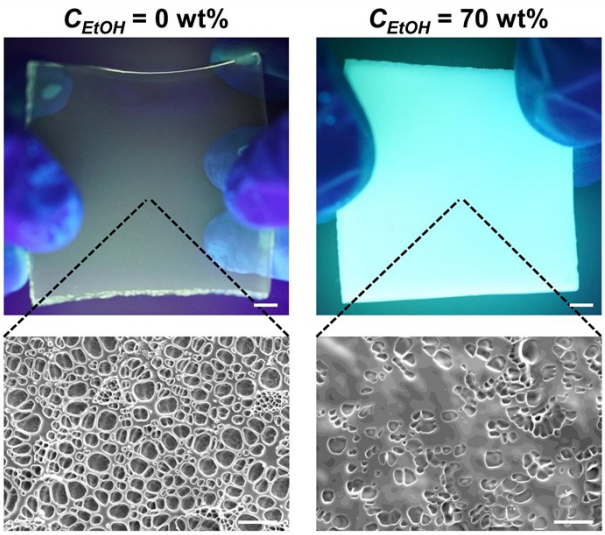

Figure S3. Different fluorescence intensity and microstructures of non-phase-separated and phase-separated PAAm gels. When containing a fluorescent molecular probe (8-anilino-1-naphthalenesulfonic acid) and exposed to ultraviolet light, the phase-separated gel (C_{EtOH} = 70%) displays strong fluorescence, in contrast to no fluorescence of the non-phase-separated gel (C_{EtOH} = 0%). SEM observation further demonstrates the aggregation of polymer chains in the phase-separated gel, compared with a homogenous loose structure of the non-phase-separated gel. Scale bars in the photographs and SEM images represent 1 cm and 50 μm, respectively.

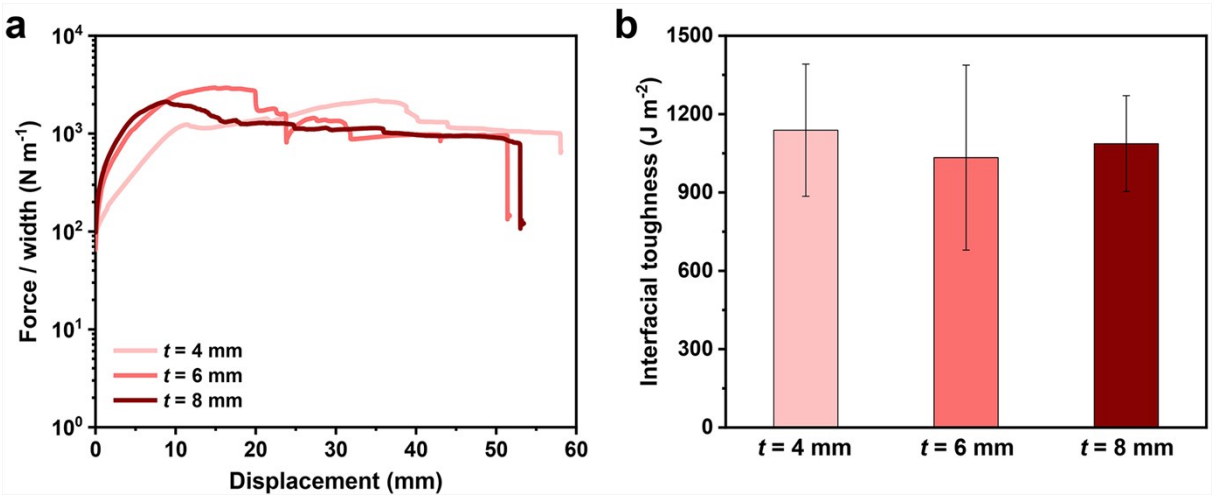

Figure S4. Interfacial toughness of PS PAAm hydrogels adhered onto a glass plate with varied sample thickness measured by 90-degree peeling tests. (a) Typical curves of peeling force per width versus displacement for hydrogel samples with a thickness of 4 mm, 6 mm, and 8 mm, respectively. (b) Measured interfacial toughness of the PS PAAm gels with different thicknesses.

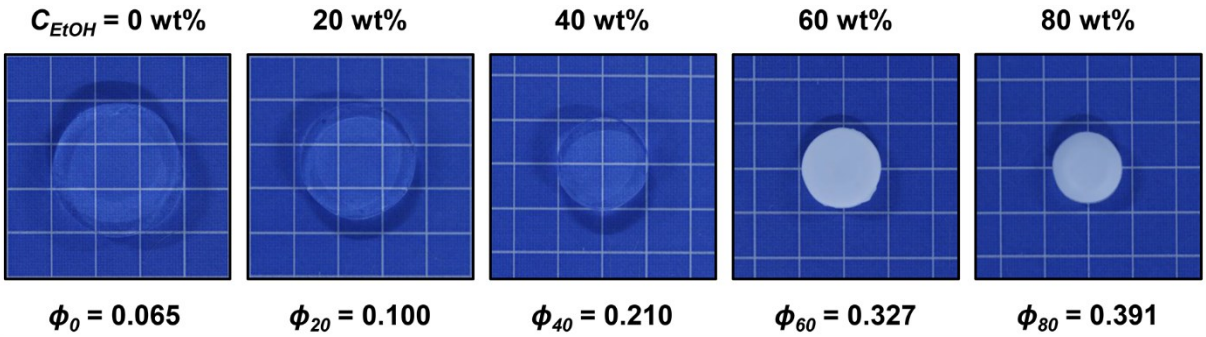

Figure S5. Influence of the C_{EtOH} on the appearance, size, and polymer volume fraction of the PAAm hydrogels. The gel gradually deswells and becomes opaque as the C_{EtOH} increases. The background grid size is 5 mm.

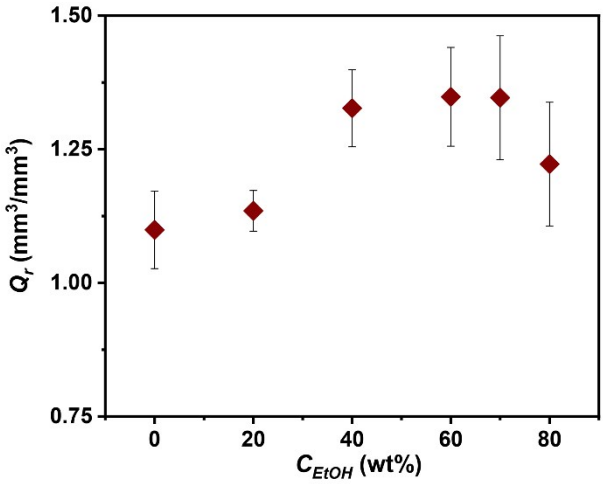

Figure S6. Relative volume-swelling ratio (Q_r) for the PAAm gel by comparing the equilibrium volume-swelling ratio of the gel in ethanol/water and ethanol/deuterium oxide mixed solvents, respectively. This term is calculated by **Equation (S5)** in the Supplementary Methods and used as a correction factor for the polymer surface density calibration.

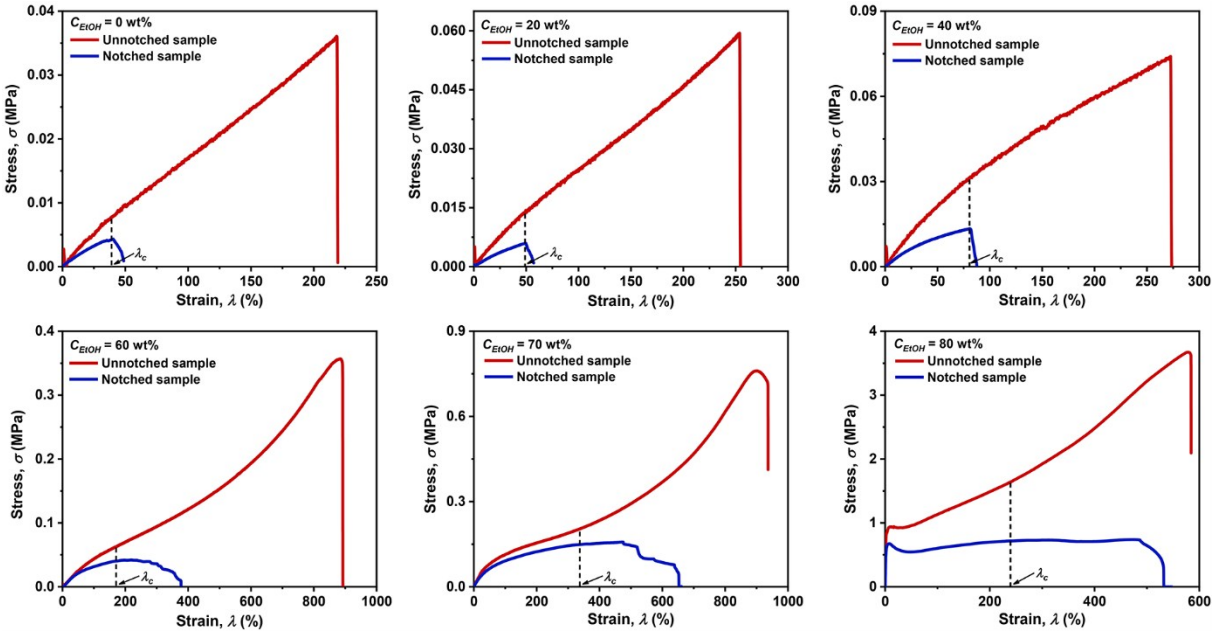

Figure S7. Stress (σ)-strain (λ) curves of unnotched and notched PAAm hydrogels that are equilibrated in ethanol/water mixed solvents with varied C_{EtOH}. λ_c represents the critical strain where the crack starts to propagate for the notched samples.

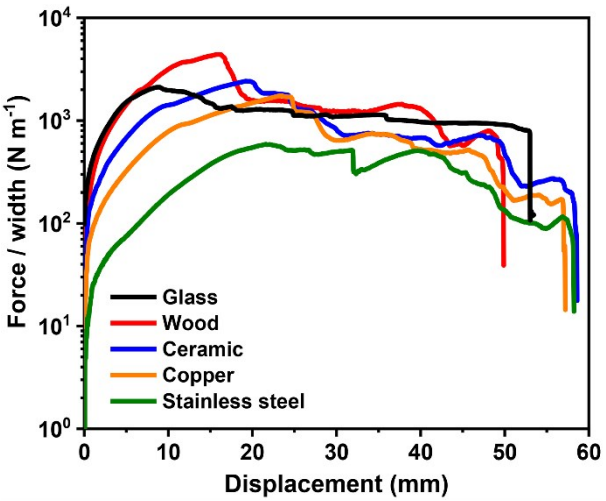

Figure S8. Typical curves of peeling force per width versus displacement for PS PAAm hydrogels adhered onto various solid surfaces. The interfacial toughness is calculated by dividing the plateau force by the width of the hydrogel.

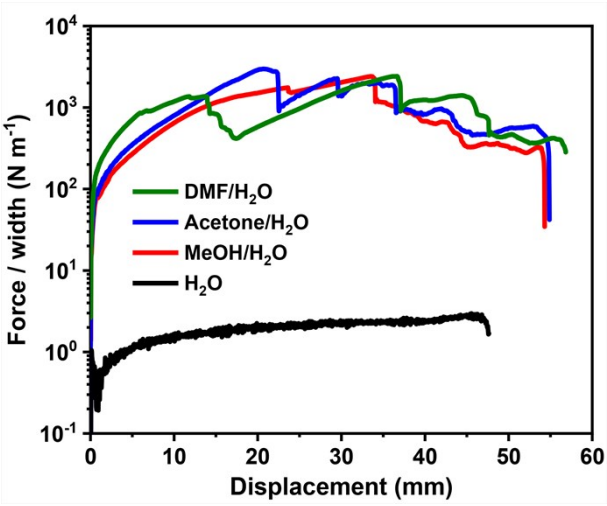

Figure S9. Typical curves of peeling force per width versus displacement for PAAm hydrogels that are equilibrated in various solvents. The PAAm gels that are equilibrated in organic/water mixed solvents show much higher peeling force per width compared with the PAAm gel that is equilibrated in pure water.

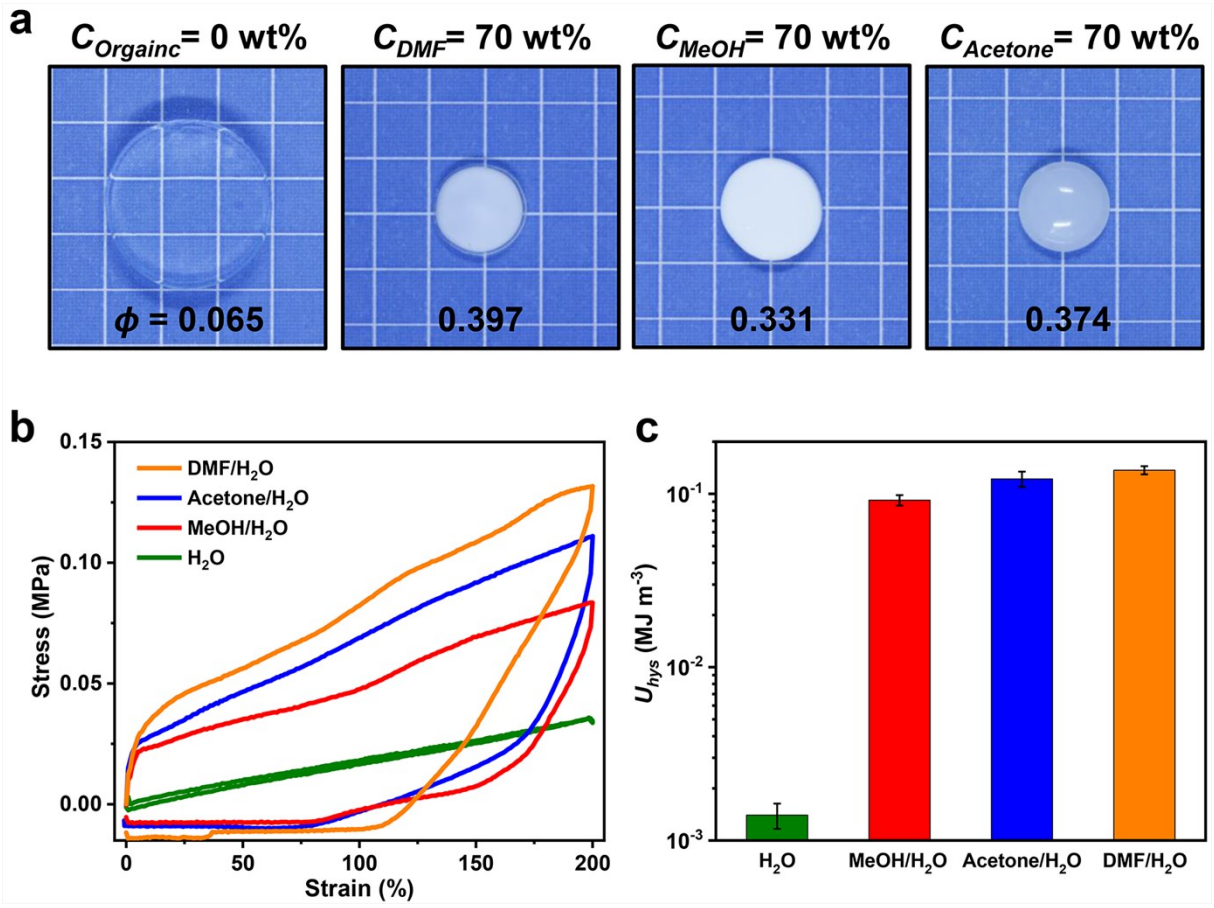

Figure S10. Phase separation of PAAm hydrogels induced by various organic/water mixed solvents. (a) Phase separation is induced when the PAAm gel is equilibrated in various organic/water mixed solvents (See the **Supplementary Methods**). All gels deswell and become opaque in the mixed solvents. Corresponding polymer volume fraction (ϕ) is also significantly increased. (b) Tensile loading-unloading stress-strain curves of the PAAm gels equilibrated in various mixed solvents compared with the original gel in water. (c) The mechanical hysteresis (U_{hys}) of the phase-separated gels in mixed solvents compared with that of the original gel in water. The energy dissipation capability is dramatically enhanced due to phase separation. The background grid size in (a) is 5 mm.

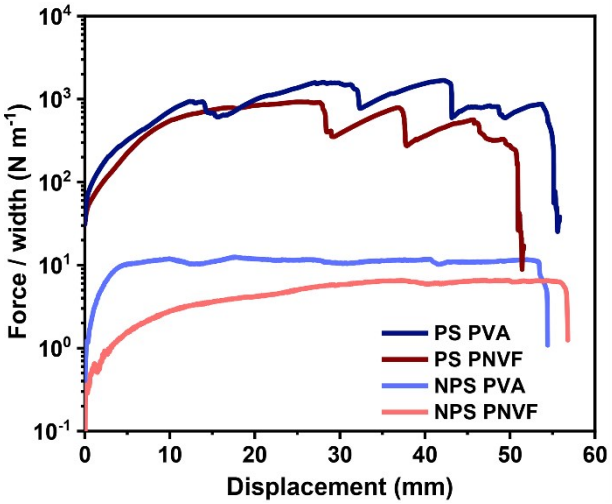

Figure S11. Contrasting adhesion performance of other types of hydrogels before and after phase separation. The PNVF and PVA hydrogels show much improved peeling force per width after phase separation in the acetone/water mixed solvent ($C_{Acetone}$ = 70 wt%).

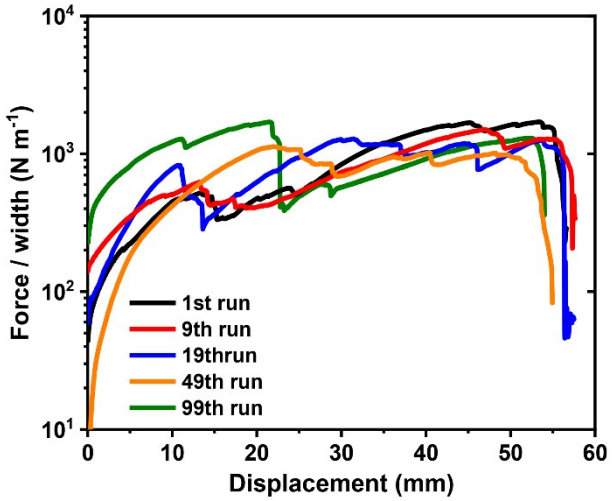

Figure S12. Repeatability of the noncovalent adhesion of the PS PAAm gel to the solid surface. The PS gel shows similar curves of peeling force per width versus displacement in 100 attach/detach cycles.

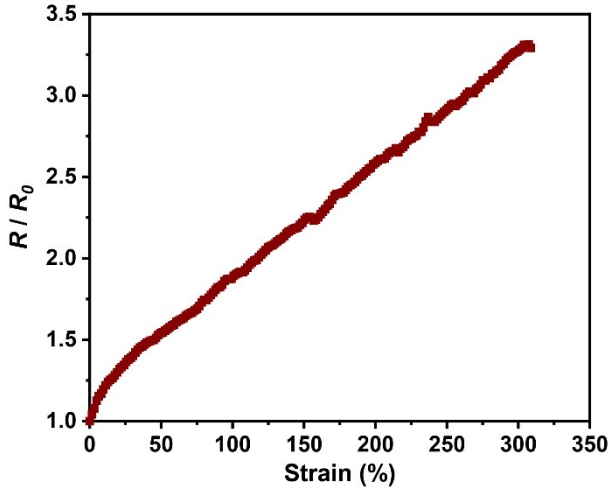

Figure S13. Strain-sensitive conductivity of the PS PAAm hydrogel containing $CaCl_2$. The gel shows a strain-dependent relative resistance (R/R_0).

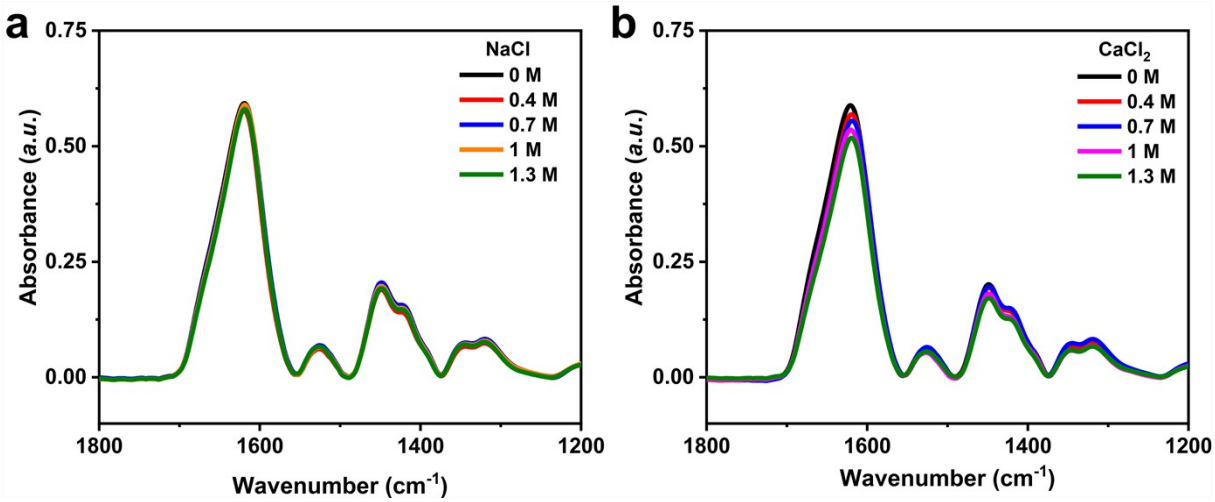

Figure S14. The infrared absorption spectra and signal intensity of the phase-separated PAAm gel (C_{EtOH} = 75 wt%) containing various concentrations of NaCl (a) and $CaCl_2$ (b), respectively.

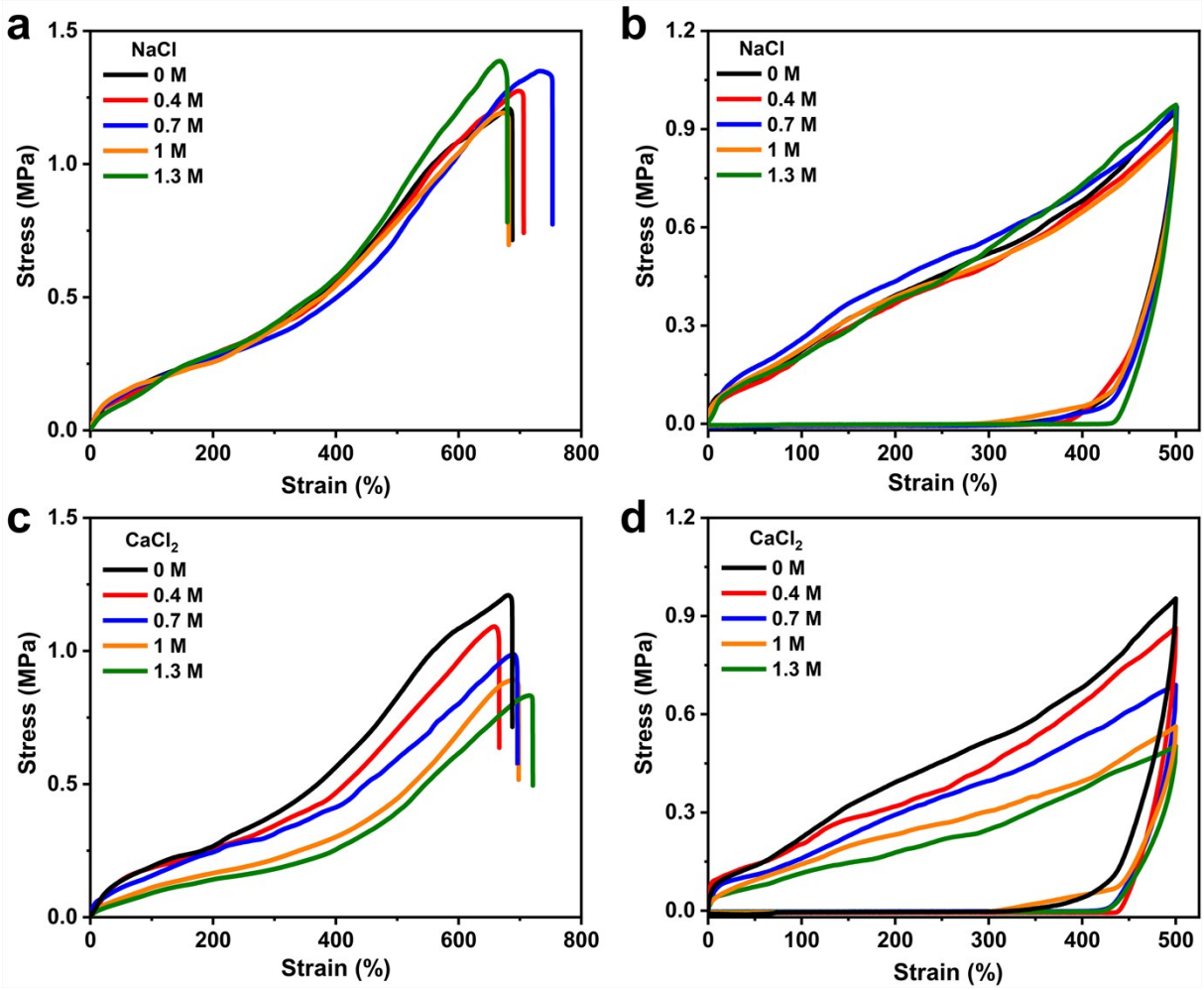

Figure S15. The bulk mechanical properties of the phase-separated PAAm gel (C_{EtOH} = 75 wt%) containing various concentrations of NaCl and $CaCl_2$, respectively. (a) and (c) gather stress-strain curves by uniaxial tensile tests. (b) and (d) display stress-strain curves by load-unloading tensile tests.

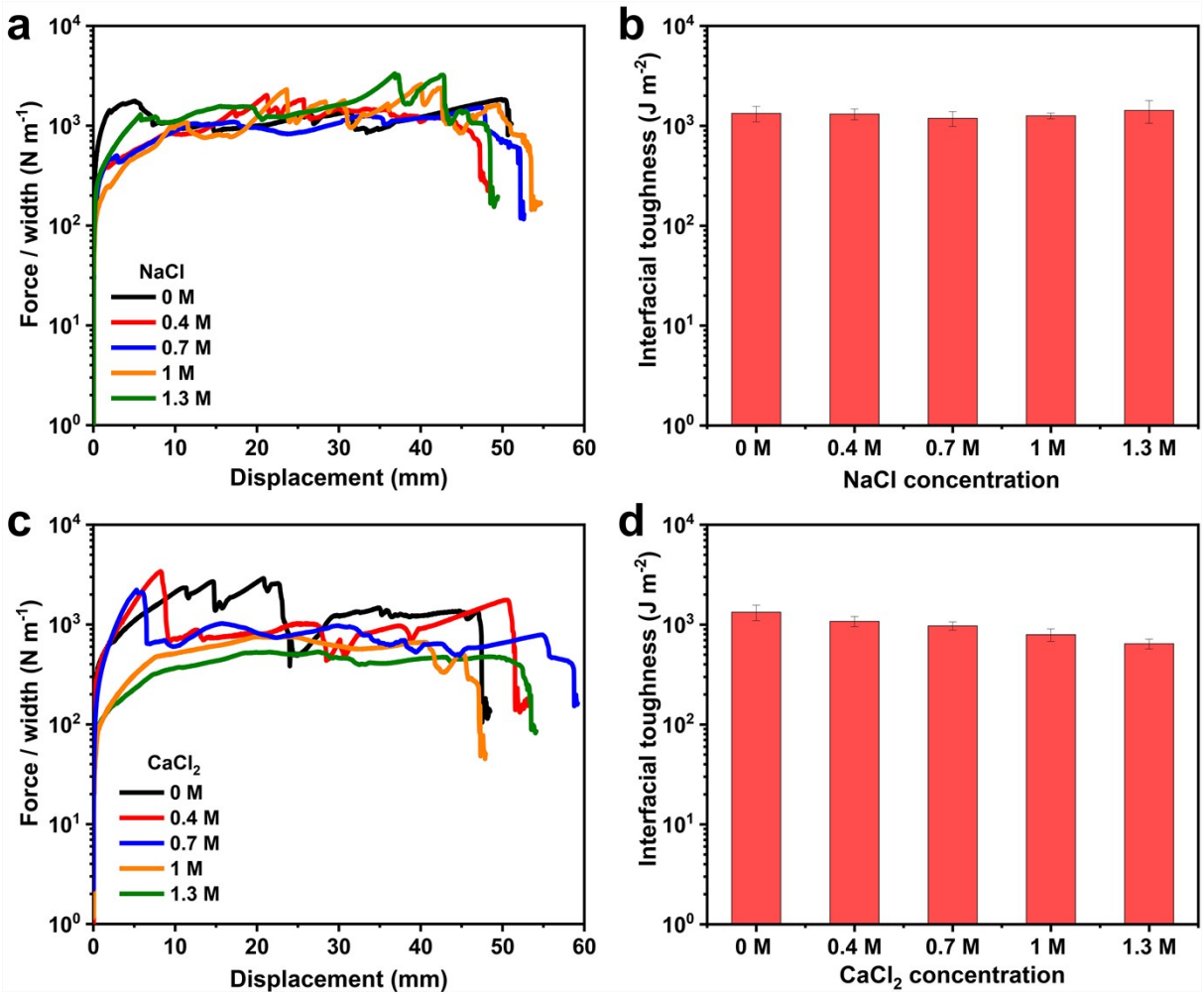

Figure S16. Adhesion properties of the phase-separated PAAm gel (C_{EtOH} = 75 wt%) with various concentrations of NaCl and $CaCl_2$, respectively. (a) and (c) are the curves of the peeling force per width of gels versus displacement. (b) and (d) are the calculated interfacial toughness.

Table S1. Summary of structural and mechanical properties of PAAm gels that are equilibrated in water and ethanol/water mixed solvents with varied C_{EtOH}. The parameters include volume-swelling ratio (Q), polymer volume fraction (ϕ), tensile fracture stress (σ), fracture strain (λ), Young's modulus (E), work of extension at fracture (W_{extf}), mechanical hysteresis (U_{hys}) at the strain range of 0-200%, and fracture energy (T). Testing velocity of the uniaxial tensile tests and pure shear tests is 100 mm min^{-1}. The strain rate of the uniaxial tensile tests is 0.14 s^{-1}. All mechanical tests were conducted at room temperature (24 ^{o}C).

C_{EtOH} (wt%)	Q	ϕ	σ (MPa)	λ (%)	E (MPa)	W_{extf} (MJ m^{-3})	U_{hys} (MJ m^{-3})	T (kJ m^{-2})
80	0.166	0.391	3.67	585	39.059	11.94	1.726	23.22
70	0.175	0.371	0.72	936	0.339	2.54	0.139	3.53
60	0.198	0.327	0.36	893	0.150	1.45	0.0047	0.68
40	0.310	0.210	0.073	273	0.049	0.12	0.0031	0.05
20	0.651	0.100	0.057	255	0.035	0.09	0.0020	0.03
0	1	0.065	0.034	219	0.025	0.04	0.0014	0.01

Supplementary Movie Captions

Movie S1: Contrasting adhesion behaviors of brittle hydrogels before and after phase separation. The phase-separated PAAm gel is highly adhesive and shows obvious hysteresis during interfacial separation, whereas the non-phase-separated PAAm gel is almost non-adhesive.

Movie S2: Universal adhesion of the phase-separated gel to various solid surfaces. Three different solid materials, a glass plate, a copper sheet, and a block of wood, can be easily glued by a phase-separated PAAm gel (15 cm × 15 cm × 0.15 cm). In contrast, a non-phase-separated PAAm gel (10 cm × 10 cm × 0.3 cm) cannot joint the solid materials.

Movie S3: A typical attach/detach cycle of a phase-separated gel to a solid substrate. The phase-separated PAAm gel (12 cm × 4 cm × 0.15 cm) shows tough adhesion to the glass substrate, while it can also be facilely removed by dropping water at the gel-solid interface. Once the gel is resoaked into the mixed solvent for a while, it restores the adhesive capacity to the solid surface.

Movie S4: Soft-rigid hybrid conductor enabled by tough phase-separated gel-solid adhesion. A stretchable conductor is fabricated by attaching a $CaCl_2$-containing phase-separated PAAm gel to copper sheets. By periodically stretching and relaxing the conductor, the brightness of the powered LED light can be easily adjusted. Such a tension/relaxation cycle to adjust the conductivity of the conductor can be repeated many times without gel-solid debonding. On the contrary, gel-solid debonding occurs when a $CaCl_2$-containing non-phase-separated PAAm gel is utilized as a joint for the conductor.

Supplementary References

1. K. Sato, T. Nakajima, T. Hisamatsu, T. Nonoyama, T. Kurokawa, J. P. Gong, *Adv. Mater.* **2015**, 27, 6990.
2. H. Yuk, T. Zhang, S. Lin, G. A. Parada, X. Zhao, *Nat. Mater.* **2016**, 15, 190.
3. R. Long, C.-Y. Hui, *Soft Matter* **2016**, 12, 8069.